

A General Concept for Highly Efficient Covalent Laser Patterning of Graphene Based on Silver Carboxylates

Tao Wei,^{a,*} Xin Liu,^b Sabrin Al-Fogra,^b Julien Bachmann,^{b,c} Frank Hauke,^a and Andreas Hirsch^{a,*}

^aDepartment of Chemistry and Pharmacy & Joint Institute of Advanced Materials and Processes (ZMP), Friedrich-Alexander University of Erlangen-Nürnberg Nikolaus-Fiebiger-Strasse 10, 91058, Erlangen, Germany

^bChemistry of Thin Film Materials, Department of Chemistry and Pharmacy, Friedrich-Alexander University of Erlangen-Nürnberg Cauerstr. 3, Erlangen 91058, Erlangen, Germany

^c Saint-Petersburg State University, Institute of Chemistry, Universitetskii pr. 26, 198504 St. Petersburg, Russia

Content

- S1. Experimental section**
- S2. 2D-patterning of graphene by laser writing**
- S3. Reference experiment: Laser writing with different wavelengths and Raman features after silver removal**
- S4. Quantifying the degree of functionalization**
- S5. Reference experiment: laser writing on multi-layer graphene**
- S6. Temperature-dependent defunctionalization of G_A , G_B , and G_C**
- S7. Removal of the silver nanoparticles**

S1. Experimental section

Materials

CVD graphene on a 1×1 cm² polymethyl methacrylate (PMMA) substrate was purchased from ACS Material Co. (USA). All other chemicals were purchased from Sigma Aldrich Co. (Germany) and used without further treatment. Si/SiO₂ wafers (300 nm oxide layer) were purchased from Fraunhofer-Institute in Erlangen. Before using, the Si/SiO₂ wafers were cleaned by immersing into isopropanol for a ultrasonic treatment (300W) for 5 min.

Raman Spectroscopy

The Raman spectroscopic characterization was performed on a Horiba Jobin Yvon LabRAM Aramis. A laser (Olympus LMPlanF150x, NA 0.50) with an excitation wavelength of 532 nm, intensity of 8 mW and a spot size of ~ 1 μ m was used. The spectrometer was calibrated by using crystalline graphite. Spectral data was obtained through a motorized x-y table in a continuous line scan mode (SWIFT-module). The temperature dependent Raman measurements were performed in a Linkam stage THMS 600, equipped with a liquid nitrogen pump MS94 for temperature stabilization under a constant flow of nitrogen. The measurements were carried out on Si/SiO₂ wafers with a heating rate of 10 K/min.

Scanning electron microscopy-energy dispersive X-ray spectroscopy (SEM-EDS)

Scanning electron microscopyenergy dispersive X-ray spectroscopy was performed on a FE-SEM (Auriga, Carl Zeiss) equipped with an oxford X-max 80. The working conditions were set at an operating accelerating voltage of 5 kV for F and 15 kV for Ag, working distance of 7.3mm, the elevation angle of the detector was 35° and the sample was vertically aligned with respect to the secondary-electron emission.

Atomic force microscopy (AFM)

Atomic force microscopy was carried out using a Bruker Dimension Icon microscope in tapping mode. Bruker Scanasyt-Air silicon tips on nitride levers with a spring constant of 0.4 N m⁻¹ were used to obtain images resolved by 1024×1024 pixels.

S2. 2D-patterning of graphene by laser writing

Based on a wet transfer technique as we described before,^{S1} the graphene monolayer was deposited on a Si/SiO₂. Afterwards, the PMMA coating was removed by a treatment with acetone vapor (60 min) and the wafer was dried in air. Subsequently, three wafers covered with the graphene monolayer were respectively immersed (ca. 30 min) into a solution of silver acetate (0.05 mmol/mL), silver benzoate (0.06 mmol/mL) and silver heptafluorobutyrate (9 mmol/mL) dissolved in isopropanol. As soon as the wafers were taken out from the solution, one drop of the silver heptafluorobutyrate solution and several drops of silver acetate, silver benzoate (considering their poor solubilities) were dropped on the respective wafer. These wafers were subsequently dried by a gentle stream of argon to give rise to the formation of films atop the graphene. The corresponding optical images of films are shown in Figure S1A, S1D, and S1G. The two covering steps are required in order to ensure the formation of a homogeneous and sufficiently thick film atop the graphene. The laser-writing of graphene was carried out in the Raman spectrometer by directly focusing a green laser (532 nm, 50× magnification of objective, irradiation time 1 s, 8 mW) on the film and this causes a laser-triggered photolysis of these photosensitizers (including silver acetate, silver benzoate, and silver heptafluorobutyrate), generating CH₃·, C₆H₅·, C₃F₇· radicals, confined to the laser-irradiated areas. These intermediately formed radicals directly react with the monolayer-graphene underneath, resulting in the generation of 2D patterns on graphene named as G_A, G_B and G_C. The resulting letter patterns of “Z” (G_A), “M” (G_B), and “P” (G_C) were written in the film as shown in respective microscopic image (Figure S1B, S1E, and S1H). After the laser-writing process, the samples were rinsed with 20 mL acetone for three times to completely remove all reactants and by-products. Besides, AFM measurements were carried out to detect the film thickness of the laser-triggered 2D-functionalized areas (Figure 2A, 2C and 2E, black square marked areas). It can be clearly seen that the film thicknesses of silver acetate, silver benzoate, and silver heptafluorobutyrate were 40, 40, and 50 nm, respectively (Figure 2B, 2D and 2F).

Interestingly, after this washing treatment, the patterns remain visible (Figure S1C, S1F and S1I). This can be traced back to the fact that silver nanoparticles have simultaneously been formed during the laser-irradiation of the silver carboxylate film. Due to the formation of silver nanoparticles and the corresponding SERS effect,^{S2,S3} the Raman G-band intensities for G_A, G_B, and G_C were significantly enhanced (30 times high) with respect to the pristine graphene sample (Figure 1).

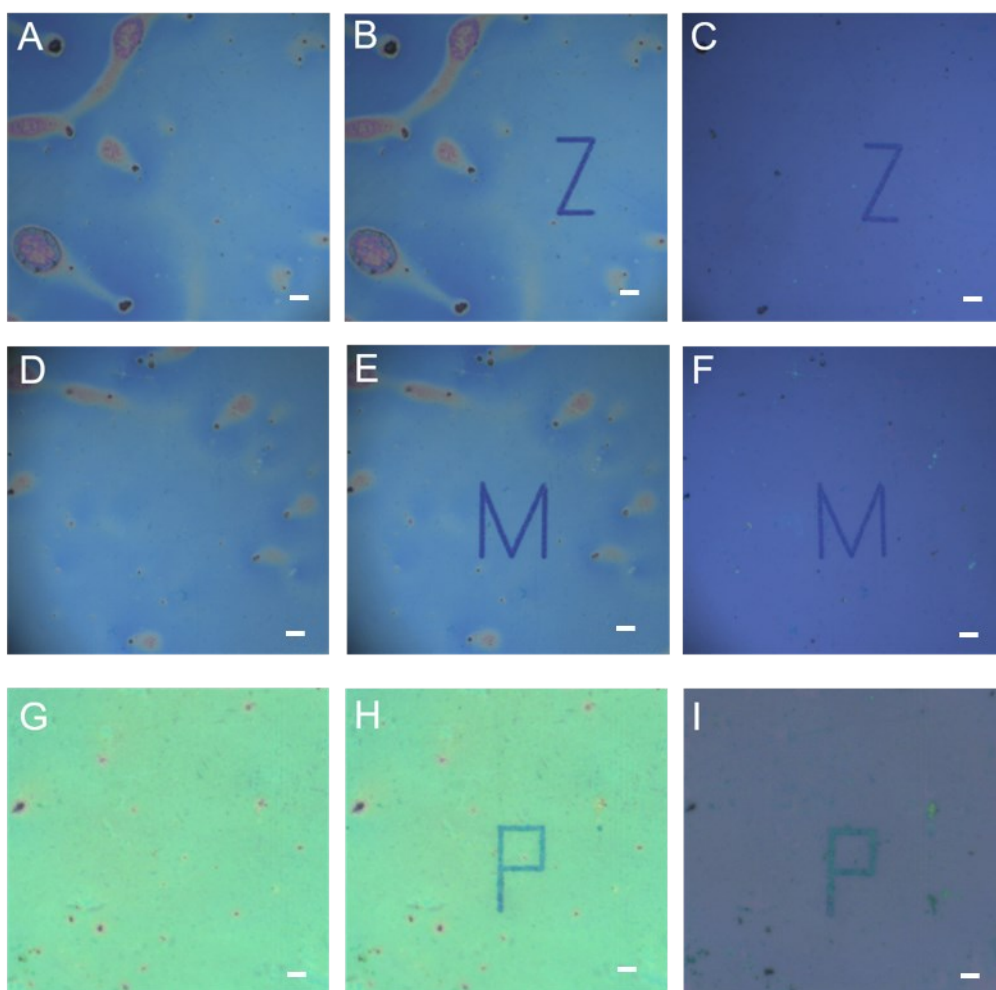


Figure S1. Optical images of (A) a film of the silver acetate photosensitizer film deposited on a monolayer graphene, (B) the same area after laser-induced reaction, and (C) after washing with acetone to remove the film and the remaining silver nanoparticles produced by decomposition of silver acetate. Analog optical information as in (A-C) given for the silver benzoate (D-F) and silver heptafluorobutyrate (G-I). Scale bar: 6 μm .

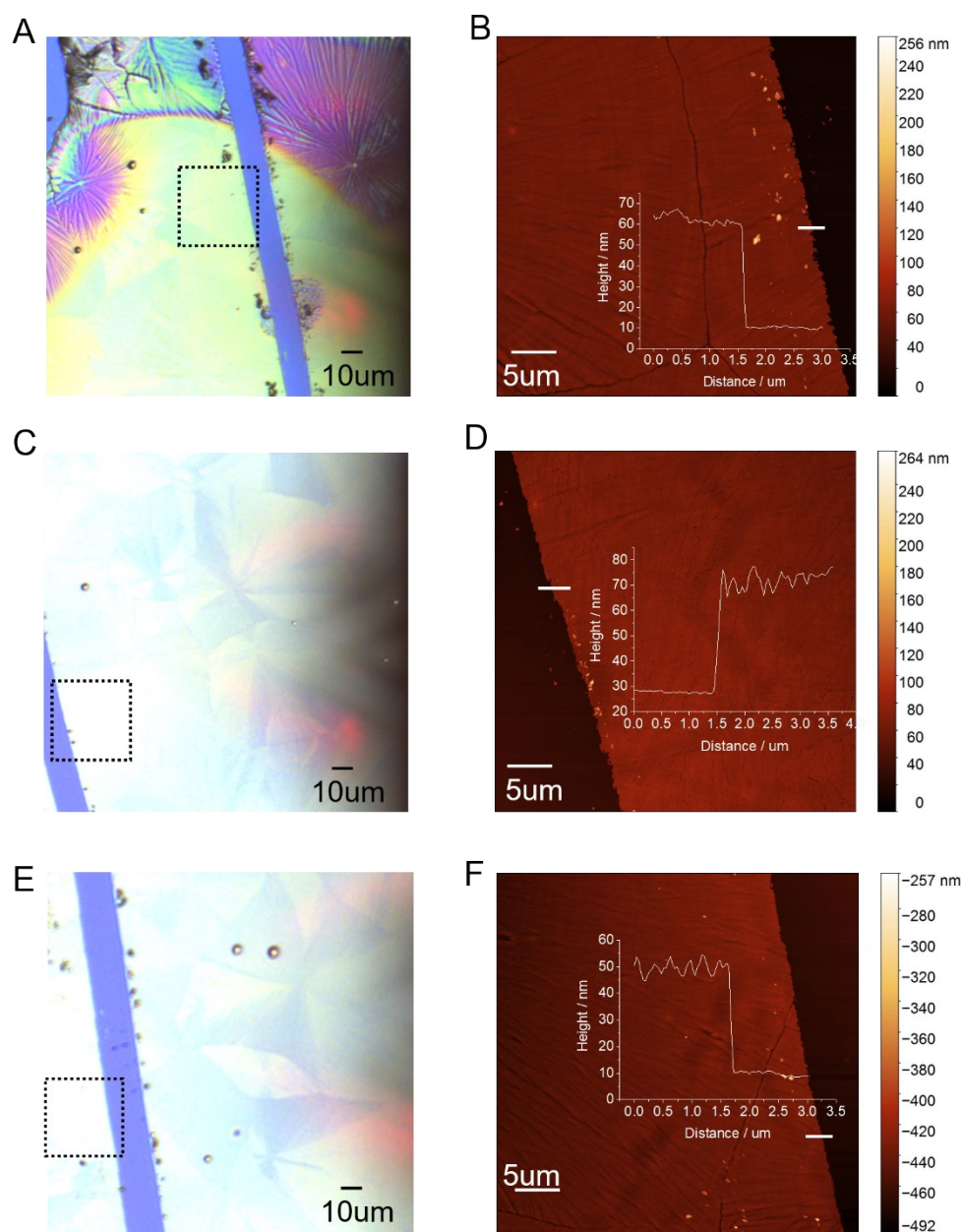


Figure S2. Optical images and corresponding AFM images of the film of silver acetate (A, B), silver benzoate (C, D), and silver heptafluorobutyrate (E, F). In order to facilitate the AFM measurements the scratches shown in image A, C, and E have been implemented on purpose. The black square denotes the location where the AFM characterization has been carried out.

S3. Reference experiment: Laser writing with different wavelengths and Raman features after silver removal

Prior to the 2D-patterning of graphene, Raman lasers with different wavelengths including 457, 532 and 633 nm have been tested to screen out the best laser for graphene 2D-patterning. Following a similar procedure, the homogeneous films of each photosensitizer comprising

silver acetate, silver benzoate, and silver heptafluorobutyrate were prepared atop the monolayer graphene deposited on a Si/SiO₂ wafer. The laser-triggered 2D-functionalizations was performed by focusing the different Raman-lasers on the respective films and the corresponding Raman spectra were recorded. Clearly, Raman spectra for the different laser wavelengths of each photosensitizer differ from each other substantially. Compared to the Raman spectra obtained under 457 and 633 nm laser irradiation, the Raman spectra generated under irradiation with a 532 nm laser (for each photosensitizer) exhibits an even broader D- and G-band as well as a almost vanished 2D-band, suggesting its higher degree of 2D-functionalization. As a consequence, the green laser (532 nm) was naturally adopted for the next 2D-pattern of graphene.

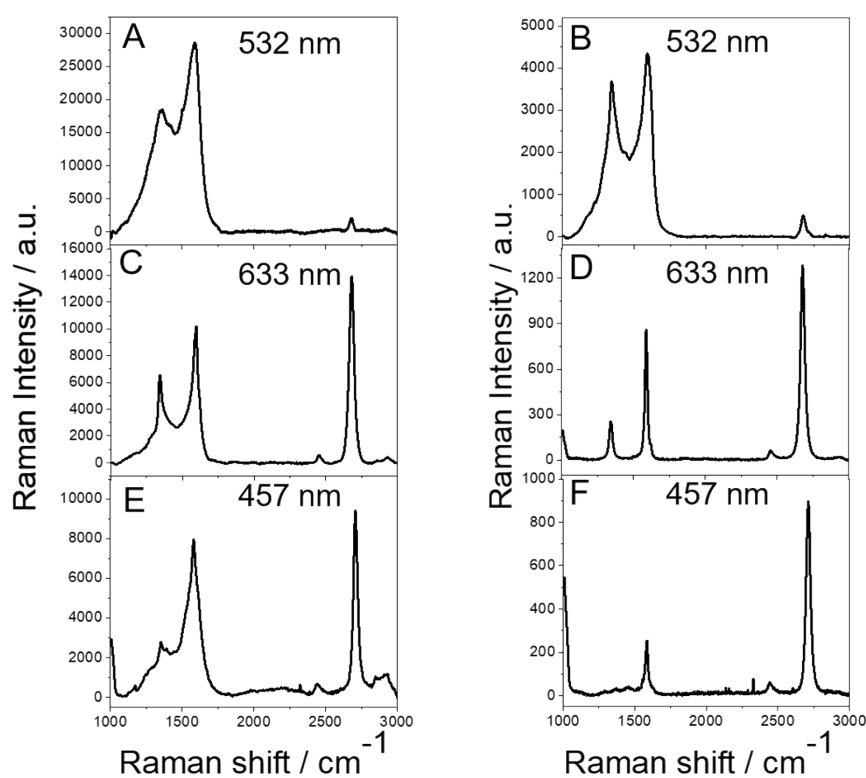


Figure S3. Raman spectra of functionalized monolayer graphene by the usage of silver acetate under irradiation of different laser wavelengths in the writing process: Left column: Before removal of the silver nanoparticles A ($\lambda_{\text{exc}} = 532$ nm), C ($\lambda_{\text{exc}} = 633$ nm), and E ($\lambda_{\text{exc}} = 457$ nm). Right column: After removal of the silver nanoparticles B ($\lambda_{\text{exc}} = 532$ nm), D ($\lambda_{\text{exc}} = 633$ nm), and F ($\lambda_{\text{exc}} = 457$ nm).

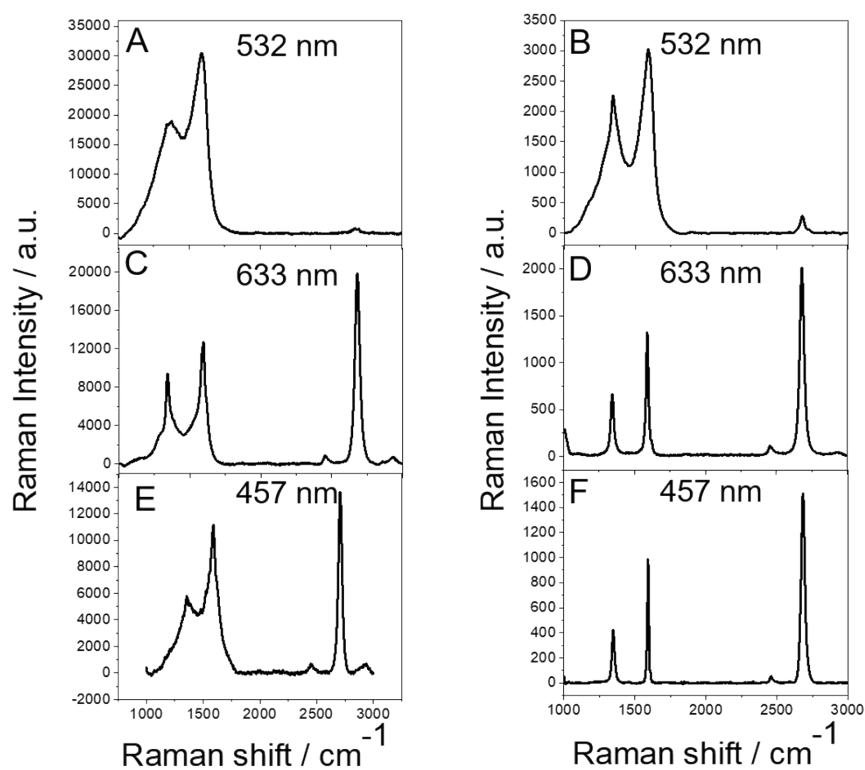


Figure S4. Raman spectra of functionalized monolayer graphene by the usage of silver benzoate under irradiation of different laser wavelengths in the writing process: Left column: Before removal of the silver nanoparticles A ($\lambda_{\text{exc}} = 532$ nm), C ($\lambda_{\text{exc}} = 633$ nm), and E ($\lambda_{\text{exc}} = 457$ nm). Right column: After removal of the silver nanoparticles B ($\lambda_{\text{exc}} = 532$ nm), D ($\lambda_{\text{exc}} = 633$ nm), and F ($\lambda_{\text{exc}} = 457$ nm).

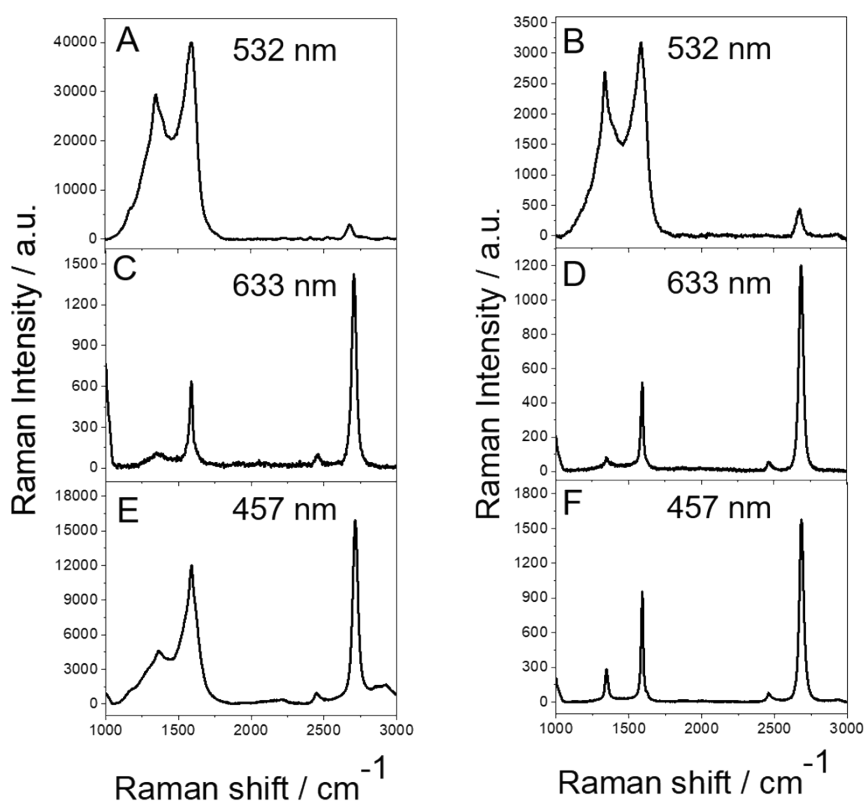


Figure S5. Raman spectra of functionalized monolayer graphene by the usage of silver heptafluorobutyrate under irradiation of different laser wavelengths in the writing process: Left column: Before removal of the silver nanoparticles A ($\lambda_{\text{exc}} = 532$ nm), C ($\lambda_{\text{exc}} = 633$ nm), and E ($\lambda_{\text{exc}} = 457$ nm). Right column: After removal of the silver nanoparticles B ($\lambda_{\text{exc}} = 532$ nm), D ($\lambda_{\text{exc}} = 633$ nm), and F ($\lambda_{\text{exc}} = 457$ nm).

As outlined in the main text, in the course of the laser-writing process, in addition to the formation of CH_3 - C_6H_5 -, C_3F_7 -radicals, silver nanoparticles were also generated and were patterned exactly in the same areas where these radicals are bound to graphene. Due to the corresponding SERS effect, the Raman signals of G_A , G_B , and G_C will be increased and broadened. To deconvolute the Raman signal of this Ag/2D-functionalized graphene composites to solely provide the Raman features of 2D-functionanlized graphene samples, these silver nanoparticles were removed following the two-step strategy including dissolving with diluted nitric acid and subsequent sonication treatment. Afterwards, the Raman measurements under each laser wavelengths including 457, 532, and 633 nm were performed in the corresponding patterns. Clearly, compared to the Raman spectra before the removal of silver nanoparticles, the intensities of the D- and G-band were significantly reduced (ca. 30 times lower) and the peak shape became sharper after the removal of the silver nanoparticles.

S4. Quantifying the degree of functionalization

The Raman I_D/I_G ratio is related to the mean defect distance L_D . Generally, with the increase of L_D , the ratio of I_D/I_G will increase first and then decrease and the maximum I_D/I_G ratio (corresponding to the $L_{D\text{-crit}}$ value) is used to distinguish the low-functionalization-regime and high-functionalization-regime. The regime where the I_D/I_G ratio is located is directly reflected by the width of the Raman bands. As a consequence, the I_D/I_G ratio together with the full width at half maximum (FWHM) can be used to quantify the degree of functionalization of graphene. The observed very broad D-band with FWHM values > 30 cm^{-1} in the Raman spectra of G_A , G_B , and G_C are indicative for their location in the high-functionalization-regime. According to the method we introduced previously,^{S4} the degrees of functionalization of G_A , G_B , and G_C can be quantified as 1.76%, 1.65 %, and 1.65%, respectively. Additionally, we also quantified the degrees of functionalization of previously reported covalent patterning of graphene for comparison (Table S1). Clearly, similar to the strategy we introduced earlier,^{S3} our present reaction sequence provides a very higher degree of functionalization and is significantly higher than other cases. Besides, this very efficient 2D-functionanlization can be easily achieved upon 1s of irradiation time, highlighting the superiority of our protocol.

Table S1: Comparison of quantified degrees of functionalization (θ) of previously reported covalent 2D-patterning of graphene and this work.

	S2	S3	S5	S6	S7	S8	S9	S10	This work
I_D/I_G	0.80	0.60	0.56	0.72	0.80	0.25	2.60/2.80	2.58/1.12/2.40	0.60/0.65/0.65
$\theta\%$	1.385	1.758	0.009	0.012	0.014	0.004	0.066/0.060	0.059/1.176/0.053	1.758/1.647/1.647

S5. Reference experiment: laser writing on multi-layer graphene

A key factor for the high degrees of functionalization of G_A , G_B , and G_C is an antaratopic addition scenario. To verify this assumption, a reference experiment has been carried out on the basis of multi-layer (3-5 layers) graphene, where only one side is available for the addend binding. In specific, under the identical conditions as described for monolayer graphene, multi-layer (3-5 layers) graphene was applied to respectively react with silver acetate, silver benzoate, and silver heptafluorobutyrate upon laser-writing. After the reaction and subsequent work-up, the samples were characterized by Raman spectroscopy. The pristine multi-layer graphene exhibits a pronounced G-band along with an indiscernible D-band. The D-band intensity is increased after the laser-induced reaction with silver acetate, silver benzoate and silver heptafluorobutyrate, respectively, suggesting laser-triggered functionalization of the multi-layer graphene. The observed broadening of D-, G- and 2D-band can be assigned to SERS effect of the formed silver nanoparticles. However, compared to monolayer graphene, where the antaratopic reaction scenario is possible, the multi-layer graphene shows an obvious 2D-band. This Raman characteristic indicates that the I_D/I_G ratios of the multi-layer graphene samples are located in the low-functionalization-regime of the Cançado curve.^{S1} This low degree of functionalization of multi-layer graphene is due to a solely supratopic addition mode.

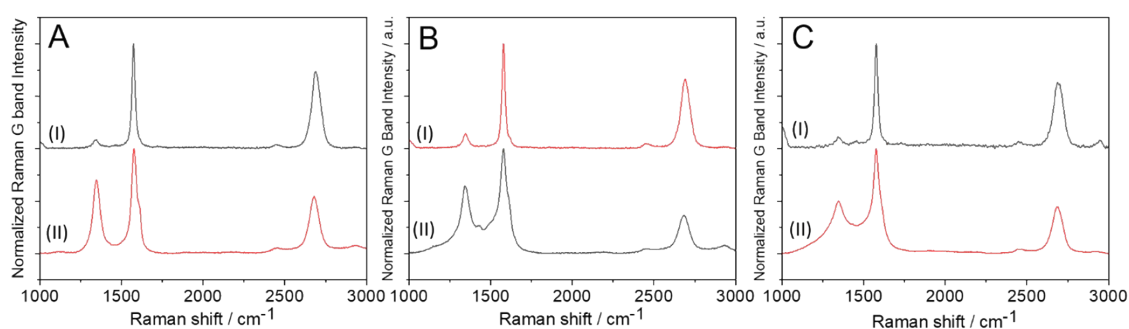


Figure S6. (A) Raman spectra of (I) pristine multi-layer graphene and (II) after laser-induced functionalization with silver acetate. (B) Raman spectra of (I) pristine multi-layer graphene and (II) after laser-induced functionalization with silver benzoate. (C) Raman spectra of (I) pristine multi-layer graphene

and (II) after laser-induced functionalization with silver heptafluorobutyrate.

S6. Temperature-dependent defunctionalization of G_A , G_B , and G_C .

The thermal-induced bond cleavage of G_A , G_B , and G_C was investigated by performing temperature-dependent Raman spectroscopy. The temperature-dependent Raman measurements (intensity of 8 mW and a spot size of $\sim 1 \mu\text{m}$) were performed in a Linkam stage THMS 600, equipped with a liquid nitrogen pump MS94 for temperature stabilization under a constant flow of nitrogen. The measurements were carried out with a heating rate of 10 K/min. In the range of 50-250 °C, the Raman data were recorded every 50 °C. In the following temperature regions (250-300 °C for G_A , 250-300 °C for G_B , 250-300 °C for G_C), where the defunctionalization of G_B and G_C occurred, we recorded the Raman data every 25 °C. Previous investigations have pointed out that along with the increase of the sp^3 -defects density, the G-band gradually widens, while the I_D/I_G ratio first increases and then decreases.^{S11, S12} Consequently, the I_D/I_G ratio combined with the G band width can provide direct information on the degree of functionalization of the covalently functionalized graphene. For sample G_B and G_C , with increasing the temperature, the I_D/I_G ratio initially increases and then decreases together with a gradual narrowing of the G-band, corroborating the assumption of a thermal-induced defunctionalization reaction (Figure S7B and 7C). In contrast, for G_A , a different thermal behavior was observed. Here, the I_D/I_G ratio together with G-band width kept almost constant as the temperature rises (up to 300 °C), indicating that no thermal induced defunctionalization reaction occurred (Figure S7A). Further increasing the temperature to 325 °C leads to the complete loss of all Raman features due to a complete degradation of the graphene framework (Figure 4B).

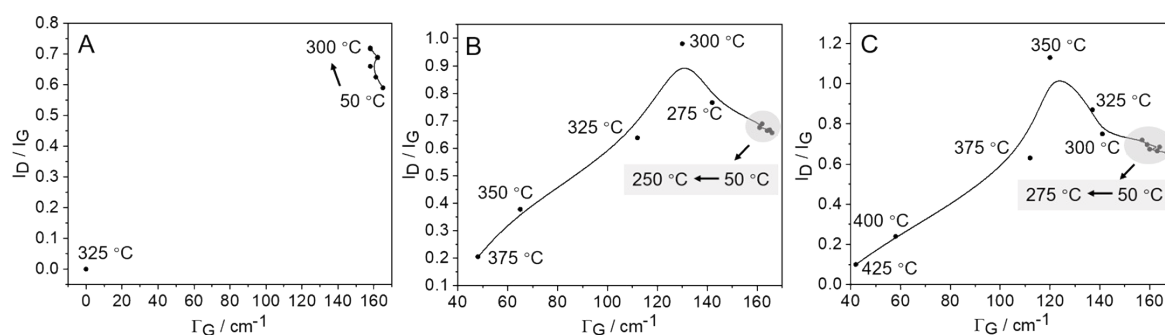


Figure S7. Correlation between the I_D/I_G ratio and the G-band width of the Raman spectra in the temperature-dependent Raman studies.

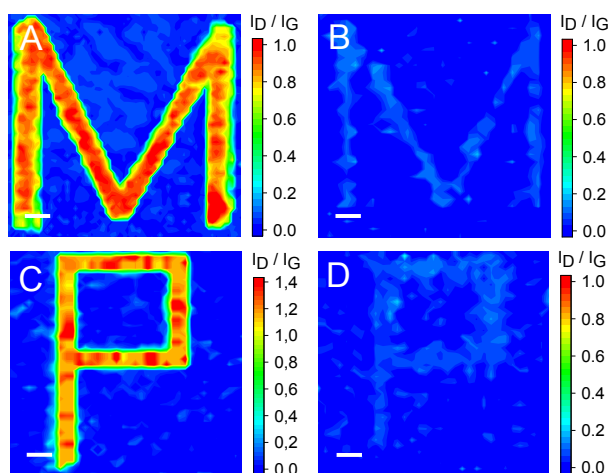


Figure S8. Raman I_D/I_G mapping image of G_B after 300 °C (A) and 375 °C (B) annealing and G_C after 350 °C (C) and 425 °C (D) annealing, $\lambda_{exc} = 532$ nm.

S7. Removal of the silver nanoparticles

Silver nanoparticles are also generated in the course of the laser-writing process. These nanoparticles are patterned exactly in the same regions where the generated alkyl/aryl radicals are bound to graphene (Figure S9A, 9D, and 9G). The formation of silver was corroborated by SEM-EDS characterization, showing a pattern-dependent distribution of elemental silver (Figure 3C). Additionally, we also employed AFM to provide a deeper insight into these Ag nanoparticles. AFM measurements clearly show a pattern-related distribution of Ag nanoparticles (Figure S10A, 10C, and 10E). These formed silver nanoparticles can be easily removed by a two-step treatment. In the first step, the samples G_A , G_B , and G_C were directly immersed into diluted nitric acid (0.3 mol/L) for 10 min. Upon this treatment, most of the silver nanoparticles were dissolved and removed (Figure S9B, 9E, and 9H). It is worth mentioning, that concentrated nitric acid should be avoided as this leads to a significant defunctionalization reaction and even degradation of the graphene structure. Afterwards, a subsequent sequential ultrasonic-treatment (ultrasonic power 30 W) of the samples immersed into diluted nitric acid (0.3 mol/L) (1 min) and isopropanol (1 min) leads to a complete removal of the Ag nanoparticles (Figure S9C, 9F, and 9I). This is also confirmed by the respective AFM measurements, where the respective letter pattern of “Z”, “M”, and “P” have completely vanished (Figure S10B, 10D, and 10F).

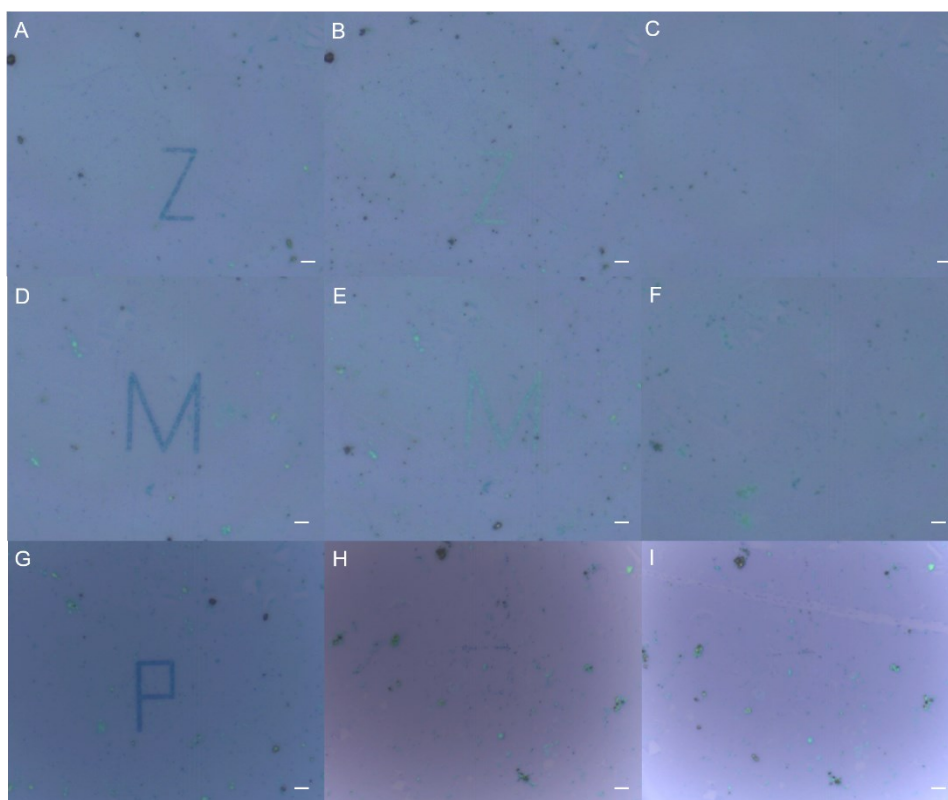


Figure S9. Optical images of covalently patterned graphene before washing - G_A (A), G_B (D), and G_C (G); after washing with diluted nitric acid - G_A (B), G_B (E), and G_C (H); ultrasonic treatment with diluted nitric acid/isopropanol for 1 min - G_A (C), G_B (F), and G_C (I). Scale bar: 6 μm .

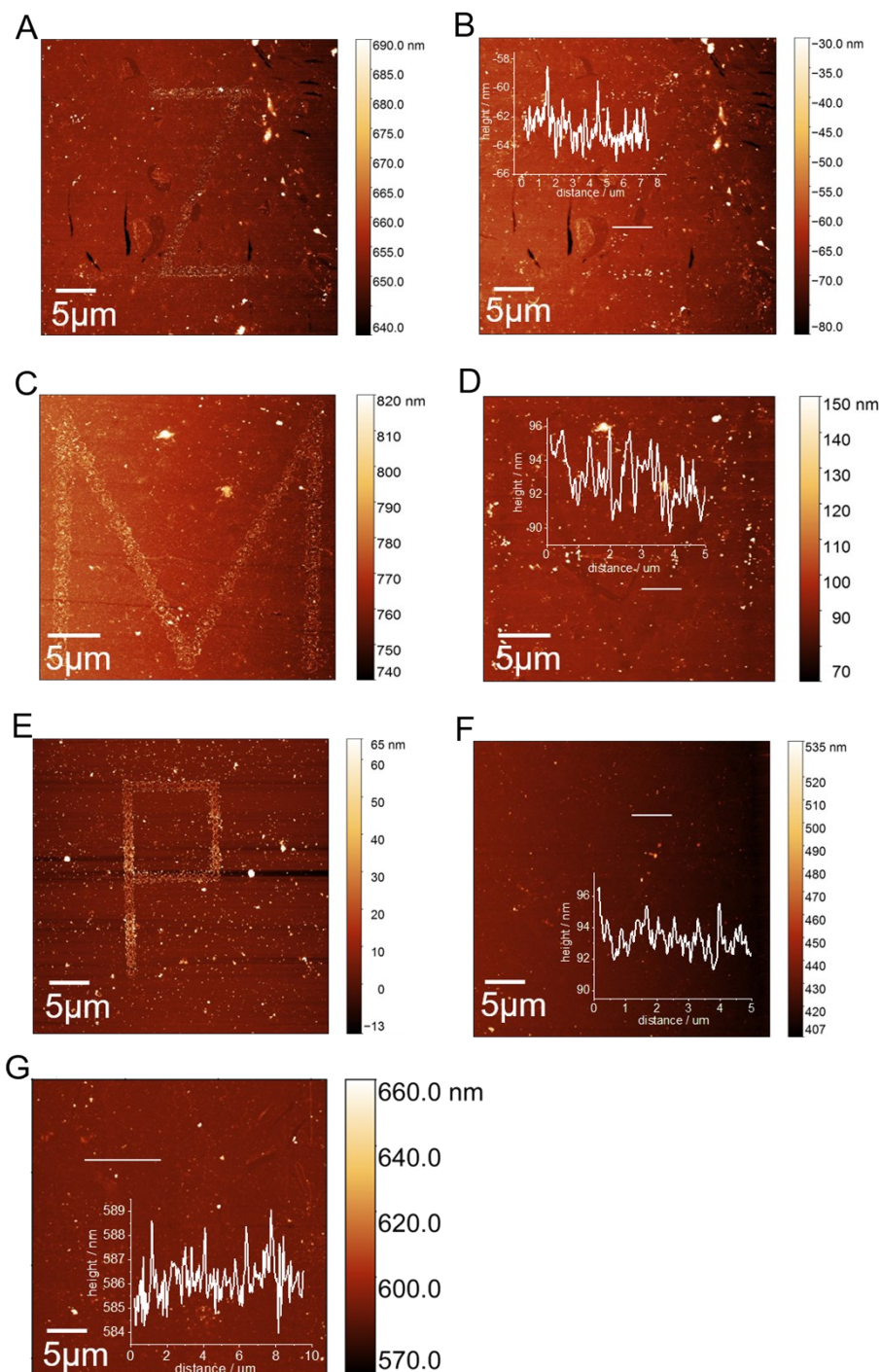


Figure S10. AMF images of the pristine graphene (G) and samples before washing - G_A (A), G_B (C), and G_C (E) - and after washing/ultrasonic treatment - G_A (B), G_B (D), and G_C (F).

References:

- [S1] Cançado L. G.; Jorio, A.; Ferreira, E. H.; Stavale, F.; Achete, C. A.; Capaz, R. B.; Moutinho, M. V. O.; Lombardo, A.; Kulmala, T. S.; Ferrari, A. C. Quantifying Defects in Graphene via Raman Spectroscopy at Different Excitation Energies. *Nano Lett.* **2011**, *11*, 3190-3196.

- [S2] Bao, L. P.; Zhao, B. L.; Lloret, V. Halik, M.; Hauke, F.; Hirsch, A. Spatially Resolved Bottom-Side Fluorination of Graphene by 2D-Substrate Patterning. *Angew. Chem. Int. Ed.* **2020**, *59*, 6766-6771.
- [S3] Wei, T.; Al-Forga, S.; Frank, H.; Hirsch, A. Direct Laser-writing on Graphene with Unprecedented Efficiency of Covalent 2D-functionalization. *J. Am. Chem. Soc.* **2020**, *142*, 21926-21931.
- [S4] Englert, J. M.; Vecera, P.; Knirsch, K. C.; Schäfer, R. A.; Hauke, F.; Hirsch, A. Scanning-Raman-Microscopy for the Statistical Analysis of Covalently Functionalized Graphene. *ACS Nano.* **2013**, *7*, 5472-5482.
- [S5] Bian, S.; Scott, A. M.; Cao, Y.; Liang, Y.; Osuna, S.; Nouk, K. N.; Brauschweig, A. B. Covalently Patterned Graphene Surfaces by a Force-accelerated Diels-Alder Reaction. *J. Am. Chem. Soc.* **2013**, *135*, 9240-9243.
- [S6] Liu, L. H.; Zorn, G. Z.; Castner, D. G.; Solanki, R.; Lerner, M. M.; Yan, M. D. A Simple and Scalable Route to Wafer-size Patterned Graphene. *J. Mater. Chem.* **2010**, *20*, 5041-5046.
- [S7] Sun, Z. Z.; Pint, C. L.; Marcano, D. C.; Zhang, C. G.; Yao, J.; Ruan, G. D.; Yan, Z.; Zhu, Y.; Hauge, R. H.; Tour, J. M. Towards Hybrid Superlattices in Graphene. *Nature Commun.* **2011**, *2*, 559-564.
- [S8] Li, J.; Li, Meng, Zhou, L. L.; Lang, S. Y.; Lu, H. Y.; Wang, D.; Chen, C. F.; Wan, L. J. Click and Patterned Functionalization of Graphene by Diels-Alder Reaction. *J. Am. Chem. Soc.* **2016**, *138*, 7448-7451.
- [S9] Wei, T.; Kohring, M.; Chen, M. C.; Yang, S. F.; Weber, H. B.; Hauke, F.; Hirsch, A. Highly Efficient and Reversible Covalent Patterning of Graphene: 2D-Management of Chemical Information. *Angew. Chem. Int. Ed.* **2020**, *59*, 5602-5606.
- [S10] Wei, T.; Kohring, M.; Weber, H. B.; Hauke, F.; Hirsch, A. Molecular Embroidering of Graphene, *Nature Commun.* **2020**, *12*, 552-560.
- [S11] Ribeiro-Soares, J.; Oliveros, M. E.; Garin, C.; David, M. V.; Martin, L. G. P.; Almeida, C. A.; Martins-Ferreira, E. H.; Takai, K.; Enoki, T.; Magalhães-Paniago, R.; Malachias, A.; Jorio, A.; Archanjo, B. S.; Achete, C. A.; Cançado, L. G. Structural Analysis of Polycrystalline Graphene Systems by Raman Spectroscopy. *Carbon*, **2015**, *95*, 646-652.
- [S12] Cançado, L. G.; Silva, M. G.; Ferreira, E. H. M.; Hof, F.; Kampuoti, K.; Huang, K.; Pénicaud, A.; Achete, C. A.; Capaz, R. B.; Jorio, A. Disentangling Contributions of Point and Line Defects in the Raman Spectra of Graphene-related Materials. *2D Materials*, **2017**, *4*, 025039-025051.